Reaction Chemistry & Engineering

High-efficiency catalytic reduction of residual oxygen for purification of carbon dioxide streams from high-pressure oxy-combustion systems

Journal:	*Reaction Chemistry & Engineering*
Manuscript ID	RE-ART-12-2020-000481.R2
Article Type:	Paper
Date Submitted by the Author:	17-Apr-2021
Complete List of Authors:	Lu, Hong; University of Illinois at Urbana-Champaign, Illinois State Geological Survey Schideman, Luke; University of Illinois at Urbana-Champaign, Illinois State Geological Survey; University of Illinois at Urbana-Champaign, Departmental of Chemical & Biomolecular Engineering Ye, Qing; University of Illinois at Urbana-Champaign, Illinois State Geological Survey Lu, Yongqi; University of Illinois at Urbana-Champaign, Illinois State Geological Survey

ARTICLE

High-efficiency catalytic reduction of residual oxygen for purification of carbon dioxide streams from high-pressure oxy-combustion systems

Received 00th January 20xx,
Accepted 00th January 20xx

DOI: 10.1039/x0xx00000x

Hong Lu,[a] Luke Schideman,[ab] Qing Ye[a] and Yongqi Lu*[a]

Pressurized oxy-combustion is a promising technology for carbon capture, utilization, and storage. For the captured CO_2 to be used for enhanced oil recovery or stored in geological formations, flue gas impurities, including residual O_2 in the CO_2 stream, must be purified to meet the purity specifications. A catalytic approach to reducing residual O_2 with CH_4 was investigated in this study. Five CoMn- and Cu-based catalysts were synthesized or acquired, and a reverse-flow fixed-bed reactor was used to assess their performance for O_2 removal from a simulated oxy-combustion flue gas at 15 bar. The impacts of the operating parameters on O_2 removal, such as temperature, gas hourly space velocity, O_2/CH_4 ratio, and gas pressure, were investigated. Among the tested catalysts, the two CoMn catalysts were superior in both activity and selectivity, with the reaction lighting off at about 350 °C and achieving 99% O_2 removal at about 500 °C. The kinetics of the catalytic reaction is discussed, and the Mars–van Krevelen redox mechanism is deemed valid for describing the reaction pathway for the top-performing CoMn catalysts. The catalytic reaction was determined to be first order in CH_4 and zero order in O_2 under the test conditions.

1. Introduction

Post-, pre-, and oxy-fuel combustion are the main technologies used for carbon capture from large CO_2 emission point sources.[1] Oxy-fuel combustion refers to the process of burning fossil fuels with pure O_2 instead of air to produce a concentrated stream of CO_2. Compared with conventional atmospheric oxy-fuel combustion, pressurized oxy-combustion can lower the costs and energy penalties by reducing equipment sizes, eliminating flue gas recirculation, and allowing for heat recovery from the flue gas.[2] The CO_2 captured from large point sources can be stored in geological formations. Interest has also been growing in utilizing CO_2 for enhanced oil recovery (EOR) to accommodate the rapid growth in world energy demand. Enhanced oil recovery has been a proven technical and economic success for more than 40 years.[3]

For CO_2 storage or EOR applications, concentrated streams of CO_2 from pressurized oxy-combustion need be purified to remove contaminants and impurities. One major impurity in oxy-combustion flue gas is residual O_2, which is required to be lower than at least 100 ppmv in such applications.[4] The removal of O_2 residuals from industrial exhaust gases has been achieved by catalytic reduction with reductants, cryogenic condensation, membrane separation, and adsorption.[5,6] The catalytic reduction of O_2 with CH_4 or other hydrocarbon reductants has advantages over other approaches because of its high efficiency and low equipment and operating complexity. Using CH_4 as the reducing gas as an example, we can simplify the O_2 reduction reaction as follows:

$$CH_4 + 2O_2 = CO_2 + 2H_2O \quad (1)$$

Multiple reactions, such as CH_4 partial oxidation and reforming, may occur, depending on the reaction conditions. The O_2 reduction reaction can be promoted with catalysts and can take place without a flame under mild temperatures between 200 and 600 °C.[7] A catalytic reaction between O_2 and CH_4 or other volatile hydrocarbon species has been used to remove either trace O_2 or residual hydrocarbons in the oil and gas, coal mining, and automobile industries.[8-10] However, the removal of percentage levels of residual O_2 under oxy-combustion conditions, especially from concentrated high-pressure CO_2 streams, has seldom been investigated. A recent study reported O_2 removal from a simulated oxy-combustion flue gas containing 3 vol % of O_2 at atmospheric pressure.[11] The authors claimed that better catalytic kinetics could be obtained at elevated pressures, but they reported no detailed work.

Cobalt-containing catalysts have been of special interest for the O_2–CH_4 reaction because of their low oxygen bond strength among nonnoble metal oxides, as indicated by the enthalpy of the formation of metal oxides divided by the number of oxygen atoms in the oxide molecule[12] and the fast rate of oxygen adsorption.[13] A few studies have shown that Co_3O_4, which consists of Co^{2+} at tetrahedral sites and Co^{3+} at octahedral sites, exhibited excellent performance in the catalytic combustion of CH_4. Zirconia-supported cobalt catalysts have been reported to exhibit the highest activity among the catalysts with various supports because their activity is enhanced by the synergic interaction between Co_3O_4 and ZrO_2.[14] Zavyalova et al.[15] studied the effects of material preparation procedures and cobalt

[a] Illinois State Geological Survey, University of Illinois at Urbana-Champaign, 615 E. Peabody Drive, Champaign, Illinois, 61820, USA. Email: yongqilu@illinois.edu
[b] Departmental of Chemical & Biomolecular Engineering, University of Illinois at Urbana-Champaign, 600 S. Matthews Avenue, Urbana, Illinois, 61801, USA
† Electronic supplementary information (ESI) available.

precursors on the reactivity of gamma-Al_2O_3-supported Co_3O_4 catalysts and found that the catalysts synthesized from equimolar redox mixtures or those with a crystallite size of about 5 nm were more reactive. A study of CH_4 combustion over Co_3O_4 made by chemical vapor deposition demonstrated that the O_2–CH_4 reaction could be described as following the Mars–Van Krevelen redox mechanism and that the reoxidation step for the catalyst was the rate-limiting step.[13] In an investigation of CoMn oxides for formaldehyde removal, the incorporation of Mn into the lattice of Co_3O_4 was credited with the enrichment of adsorbed oxygen species and a resulting improved reducibility at low temperatures.[16] Copper-containing catalysts also received attention for the O_2–CH_4 reaction in this study because of their low oxygen bond strength[12] and their high selectivity toward full conversion of the CH_4 to CO_2 without the formation of CO.[17] Our recent work has demonstrated that the activity of Cu-based catalysts for the O_2–CH_4 reaction at atmospheric pressure was due to the dynamic core-shell structure (Cu@CuO_x), whereas fully oxidized copper (CuO) present at high O_2/CH_4 ratios tended to be inactive for the reaction.[18] However, the lack of catalysts that readily fit the need for residual O_2 removal from high-pressure, CO_2-rich oxy-combustion flue gas and the high activity or selectivity that Co- or Cu-based catalysts have exhibited for CH_4 oxidation prompted our interest in these types of catalysts in the present study.

Fixed-bed reactors are widely used for heterogeneous catalytic conversion reactions in the chemical industry. Among the different types of fixed-bed reactors, a reverse-flow fixed-bed (RFFB) reactor is of special interest for catalytic processes requiring heat recovery and integration. The RFFB reactor presents a forced, unsteady-state operation that uses a fixed bed of catalyst placed between two beds of inert heat-trapping materials. The gas flow direction periodically swings from one end to the other, enabling a rather simple periodic reversal of cold gas flow to a preheated inert fixed bed. The combination of a chemical reaction and regenerative heat exchange in such a single reactor defines the uniqueness of the RFFB process, which has been applied for the incineration of wastes to remove volatile organic compounds, SO_2 oxidation, and selective reduction of NO_x in the industry.[19] Detailed reviews of the RFFB technology can be found elsewhere.[19-22] One prominent feature of the RFFB reactor is that two inert beds on either side of the catalyst bed serve as heat exchange media that store and transfer the released reaction heat to the cold feed gas, which allows the reaction to be maintained at an elevated temperature without additional gas preheating requirements.[19]

The present work investigated the performance of five CoMn oxide- and Cu-based catalysts for the reduction of residual O_2 with CH_4 from a simulated, pressurized oxy-combustion flue gas in a laboratory RFFB. The impacts of important operating parameters such as temperature, pressure, and gas partial pressure on O_2 removal were examined experimentally. The kinetics and mechanism of the catalytic reaction between O_2 and CH_4 are discussed based on the experimental results.

2. Experimental

2.1 Materials

Table 1 Cobalt- and copper-based catalysts investigated for O_2 reduction by CH_4

Catalyst	E_a (kJ/mol)	Synthesis method
$Co_{40}Mn_1$ (molar ratio)	81	Synthesized by coprecipitation; Size of 60–100 mesh; Oxidized in air before use.
$Co_{20}Mn_1$ (molar ratio)	91	Synthesized by coprecipitation; Size of 60–100 mesh; Oxidized in air before use.
Cu 20 wt %/ Al_2O_3	99	Synthesized by incipient wetness impregnation; Size of 60–100 mesh; Reduced by H_2 before use.
Cu 29 wt %/ Al_2O_3	108	Synthesized by incipient wetness impregnation; Size of 60–100 mesh; Reduced by H_2 before use.
Cu 58 wt %/ ZnO-Al_2O_3	91	Purchased from Alfa Aesar; Size of 3.7–5.5 mm; Reduced by H_2 before use.

Five catalysts (Table 1), namely two cobalt- and three copper-based materials, were investigated for the removal of residual O_2 using CH_4 as a reductant. The two cobalt-based catalysts were cobalt oxides doped with manganese oxides (abbreviated as $Co_{40}Mn_1$ and $Co_{20}Mn_1$ to represent the Co-to-Mn atomic ratios of 40:1 and 20:1 in the catalysts, respectively) and were synthesized by coprecipitation of cobalt and manganese hydroxides, followed by calcination in air. Note that the ratios of Co to Mn were preselected as a result of our prescreening studies for pure Co and CoMn catalysts, with ratios varying from 50:1 to 5:1. Two copper-based catalysts supported on gamma-alumina (abbreviated as Cu 20 wt %/Al_2O_3 and Cu 29 wt %/Al_2O_3 to represent a nominal 20% and 29% wt % of Cu in the reduced catalysts, respectively) were synthesized by incipient wet impregnation.[23] In addition, a commercial Cu-based catalyst, 63.5 wt % of CuO supported on ZnO and alumina (Alfa Aesar), was tested for comparison after being reduced in H_2 to form elemental copper (hereafter abbreviated as Cu 58 wt %/ZnO-Al_2O_3).

2.2 Experimental Setup

A laboratory, high-pressure RFFB reactor system (Fig. 1) was built for the experiments of catalytic O_2 removal from a simulated oxy-combustion flue gas. This system can be run in a reverse-flow mode or a one-direction flow mode. The reactor is a 1-in. nominal diameter and 2.5-ft-long schedule #80, 316 stainless steel pipe. The middle section of the reactor is a catalyst zone. Alumina beads (Alfa Aesar, 1/8-in. pellets) are used as a heat-trapping material placed on each side of the catalyst zone, each with a packing height of approximately 1 ft. Alumina has a high specific heat capacity (e.g., 775 J/kg·°C at 25 °C); thus, alumina beads were selected to store heat during the operation. The flow rate and composition of the simulated flue gas were controlled by individual gas mass flow controllers, and the reactor was maintained at a constant pressure by using a back-pressure controller. Solenoid valves on the gas inlet and outlet lines were operated synchronically by a programmable controller to alternate the gas flow direction periodically at a preset frequency

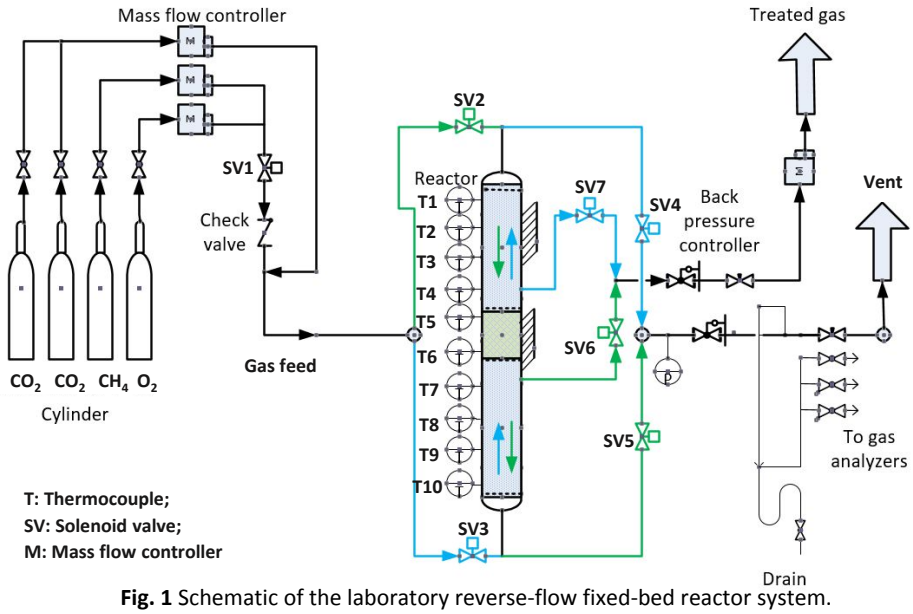

Fig. 1 Schematic of the laboratory reverse-flow fixed-bed reactor system.

(e.g., 1/240 Hz), reversing the gas flow direction as directed. The reactor was equipped with 10 thermocouples (TC1 to TC10), which were evenly distributed from the top to the bottom of the tubular reactor to measure the temperature profile. Three electric heating tapes were attached individually to the upper section of alumina beads, the middle section of the catalyst bed, and the lower section of alumina beads. Heat supplies from the heating tapes were controlled by two Variac transformers for the two alumina bead sections and by a programmed temperature controller for the catalyst bed. During the warmup stage of an experiment, the two heating tapes on the alumina bead beds were automatically turned on or off, synchronizing with the open or closed solenoid valves on the gas inlet and outlet lines in such a way that at a given moment, only the heating tape on the alumina bead bed upstream from the catalyst bed would be powered on to provide heat to preheat the feed gas to approximately 200 °C. After the system was warmed up, the heating tapes on both alumina bead beds were powered off and the operation was autothermal as the alumina bead bed downstream from the catalyst bed trapped the heat from the hot exhaust flue gas to preheat the feed gas in the following cycle. The heating tape around the catalyst bed was kept on and heat inputs were adjusted to maintain the reaction at the required temperatures to simulate different autothermal conditions without adjusting the feed or operating conditions, for convenience during laboratory testing. The concentrations of CH_4 and CO in the effluent stream were measured by an infrared dual gas analyzer (Yokogawa IR202). The oxygen concentration was determined by a Siemens Ultramat/Oxymat 6E gas analyzer. A residual gas analyzer (RGA, MKS Cirrus 2) was also used to monitor the gas composition, such as H_2, as necessary. Gas streams withdrawn for gas analysis were cooled to 4 °C to reduce the water content before they entered the analyzers, and their flow rates were controlled by individual mass flow controllers.

In a typical experiment, 50 cm^3 of catalyst was loaded to the catalyst zone between TC5 and TC6 (approximately 4 in. in height). Alumina beads were placed below and above the catalyst bed. The simulated oxy-combustion flue gas feed contained 3 vol % of O_2 with CO_2 as the balance gas. A predetermined amount of CH_4 was mixed into the flue gas to give a stoichiometric O_2/CH_4 ratio. A gas hourly specific velocity (GHSV) of ~18,000 h^{-1} (by volume under standard conditions) was mostly used. The pressure of the system was maintained at 15 bar (absolute) during the run. The temperature of the catalyst section was first increased to 200 to 250 °C and then ramped up by approximately 25 or 50 °C at each isothermal measurement step until the conversion of O_2 in the feed gas neared completion. The temperature profile along the tubular reactor height and the CH_4 and O_2 concentrations of the effluent gas stream were monitored continuously and recorded during each run. A full cycle time of 4 min was adopted to allow for the development of a relatively uniform temperature profile throughout the reaction zone. A longer cycle time would have led to a greater temperature gradient, and a shorter cycle time would have required more frequent switching of the gas direction, thus affecting the purity of the production gas stream during the flow transition time. In a few experiments, the O_2/CH_4 ratio in the feed gas was varied to be lower or higher than the stoichiometric ratio of 2. Accordingly, the O_2 concentration ranged from 1.5% to 3.75% and the CH_4 concentration ranged from 1.2% to 2.0%. Experiments were conducted at a GHSV of either 18,000 or 6,000 h^{-1}. To investigate the effect of pressure on the reaction, two other operating pressures (i.e., 1 and 5 bar) were tested. For comparison purposes, one-direction flow experiments were also conducted. During the one-direction operation, the heating tape upstream of the catalyst bed was used to continuously preheat the feed gas during the entire operation.

2.3 Catalyst Characterization

All the catalysts before and after the RFFB experiments were analyzed by X-ray diffraction (XRD; Siemens/Bruker D5000 XRD) with Cu Kα (λ = 0.15418 nm) radiation (40 kV, 30 mA). Diffraction peaks were measured by step-scanning from 10° to 100° at a speed of 0.75°

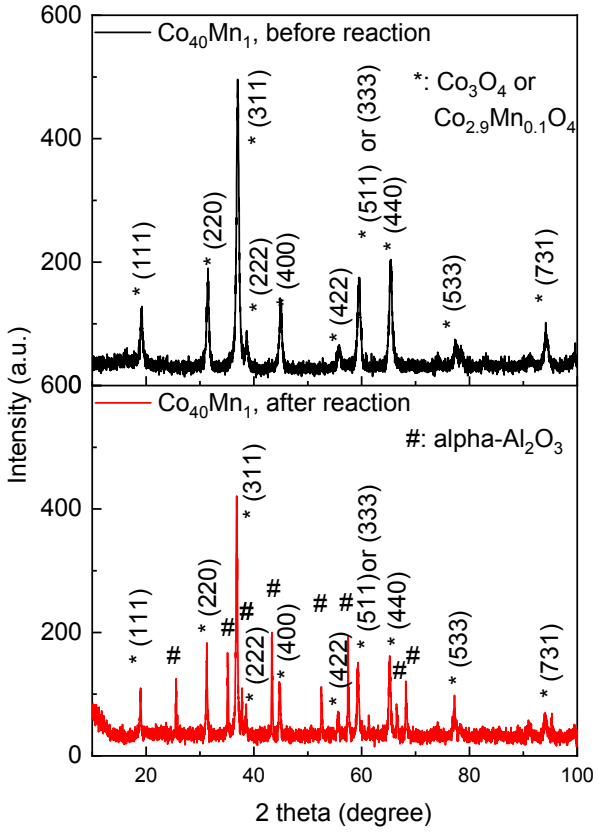

Fig. 2 X-ray diffraction patterns of $Co_{40}Mn_1$ before and after exposure to the catalytic reaction.

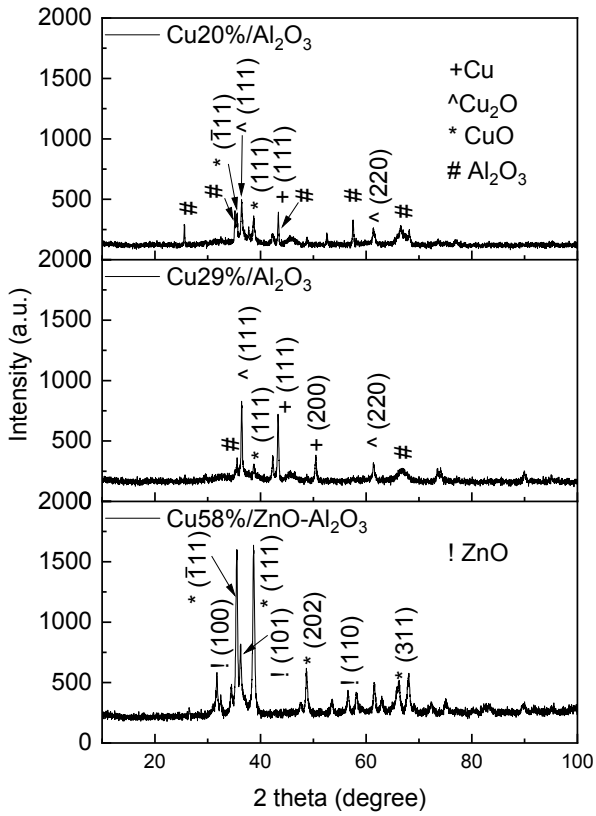

Fig. 3 X-ray diffraction patterns of Cu/Al_2O_3 catalysts after exposure to the catalytic reaction.

per minute and a step width of 0.02°. The catalysts were subjected to O_2 reduction reactions with CH_4 at various temperatures up to approximately 650 °C, for a total duration of 15 to 30 h. The oxidation states and cation distributions of the spinel structure in the Mn–Co–O system were determined by using Jade+ software (Materials Data, Inc.). In addition, Brunauer–Emmett–Teller (BET) surface areas were determined by N_2 adsorption/desorption isotherms with a surface analyzer (Micromeritics, Gemini VII).

3. Results and Discussion

3.1 Active Components of the Catalysts

X-ray diffraction spectra of the $Co_{40}Mn_1$ (before and after the reaction) and Cu-based catalysts (after the reaction) are displayed in Figs. 2 and 3, respectively. Spectra of the $Co_{20}Mn_1$ and fresh Cu-based catalysts are shown in Figs. S1 and S2 in the Supplementary Information (SI). It is evident from the figures that the preparatory conditions greatly affected the distribution of the cationic oxidation states among different crystallographic sites.[24-26] Rios et al.[27] suggested that $Co_xMn_{3-x}O_4$ could be formed for all CoMn samples prepared by the thermal decomposition of nitrate precursors. Shi et al.[16] reported that Co and Mn formed solid solutions rather than individual cobalt and manganese oxide phases even when the Mn/Co molar ratio reached as high as 1:2. Thus, Mn tends to be incorporated into the lattice of Co_3O_4, resulting in the formation of solid solutions of $Co_xMn_{3-x}O_4$, in which the value of *x* depends on the Mn/Co ratio. This atomic distribution formula was accepted in this study because a similar material preparation approach was used.

The XRD patterns for $Co_{40}Mn_1$ could be represented by $Co_{2.9}Mn_{0.1}O_4$ (JCPDS card no. 01-084-4035) and Co_3O_4 (JCPDS card No. 01-078-1969), whereas those for $Co_{20}Mn_1$ could be represented by $Co_{2.8}Mn_{0.2}O_4$ (JCPDS card no. 01-084-4036) and Co_3O_4. As shown in Table S1 of the SI, the peak positions of $Co_{40}Mn_1$ and $Co_{20}Mn_1$ after calcination in air for activation prior to the reaction shifted approximately 0.1–0.2° to lower degrees from that of Co_3O_4 at a 2θ of 65.2°, confirming the formation of the $Co_xMn_{3-x}O_4$ solid solution. Because of the nature of the solid solutions, XRD patterns for different $Co_xMn_{3-x}O_4$ species could not be differentiated. For both CoMn catalysts, no CoO or Co_2O_3 was observed based on peak deconvolution and fitting of the XRD spectra with Jade+ software (Fig. 2). Among the various cobalt oxides, Co_3O_4 and CoO were the more stable species,[28] whereas Co_3O_4 began to reduce to CoO at 750–850 °C.[29] As for Mn species in the catalysts, neither MnO_2 nor other Mn_xO_y oxides were discernible from the XRD spectra. The absence of Mn_xO_y formation was not surprising because the Mn/Co ratio was quite low (i.e., 1:20 or 1:40) in these CoMn catalysts and the small amount of Mn was completely incorporated into the CoMn oxide solid solution.

As shown in Fig. 2, the XRD peaks of the spent CoMn catalyst became narrower in comparison with those before use. The results indicated increases in crystallite size and decreases in dispersion degree, but without apparent particle sintering during the reaction.[14] A comparison of half peak widths at a 2θ of 37° suggested that the

crystallite size of $Co_{40}Mn_1$ had increased by 70%, from 16 nm to 27 nm, according to the Scherrer equation, after exposure to the CH_4 and O_2 reaction for approximately 25 hours (Table S2).

For the Cu/Al_2O_3 catalysts, the fresh samples, which were treated with H_2 reduction before use, contained only elemental Cu species, as shown in Fig. S2. After the catalyst was exposed to O_2 during the reaction, a combination of Cu, Cu_2O, and CuO were present in the XRD patterns (Fig. 3). A broad peak at a 2θ of 67° in the XRD patterns for $Cu20\%/Al_2O_3$ and $Cu29\%/Al_2O_3$ might be related to the gamma-Al_2O_3 support (Fig. S3). The transformation of Cu to Cu_2O and CuO was expected because the oxidation occurred at a high temperature. Unreacted O_2 could be present if its conversion was not complete or if more than a stoichiometric amount of O_2 was introduced in the feed gas. The amount of Cu_2O or CuO depended on the time the catalyst was exposed to the unreacted O_2 under the reaction conditions. Samain et al.[30] reported that alumina nanoparticles could form 2- to 3-nm thin flakes that stacked randomly. The disoriented thin layer of flakes may have led to an overall elusive diffraction for gamma-Al_2O_3, as shown in Fig. 3.

3.2 Temperature Profiles in the Reactor

To study the catalytic O_2–CH_4 reaction at different temperatures, the reaction temperature was increased stepwise and then stabilized at each set point for approximately 30 min. The temperature profiles of the tubular reactor at several temperature steps during the typical reverse-flow operation are presented in Fig. 4. In addition, an inset graph is included in Fig. 4 to exemplify the periodic change in the temperature profiles. For comparison purposes, those during the representative one-direction flow operation are displayed in Fig. 5.

As can be seen from Fig. 4, the temperature profiles under the reverse-flow operation are bell-shaped and symmetrical on the two sides of the catalyst zone where the temperature was the highest. The temperature profiles along the tubular reactor oscillated with the cyclic swing of the gas flow direction. The observation that the temperature dropped dramatically in each alumina bed toward the end of that side suggested that the heat was effectively trapped in one bed while that stored in the other was recovered effectively to heat the incoming cold feed gas. Such heat would otherwise need be recovered with a gas–gas heat exchanger, which tends to be large in size and ineffective for heat transfer. An approximate heat balance estimation confirmed that for the present setup, the amount of heat trapped by the alumina beads was on the same order as the external heat supplied by the electric heating tapes under the one-direction flow operation. In comparison, the temperature profiles under the one-direction flow operation were not symmetrical, and the heat front moved downward with the flow of the hot reaction gas (Fig. 5).

The temperature was also more uniform in the catalyst bed under the reverse-flow operating mode. For example, during the reverse-flow experiment (Fig. 4), the temperature difference between T5 and T6 remained at <15 °C during most of the experiment. By contrast, during the one-direction flow experiment (Fig. 5), the temperature difference between T5 and T6 was greater, up to approximately 100 °C. It can clearly be seen that the periodic reversal of the gas flow direction prevented the development of a steady temperature gradient across the catalyst bed from the exothermic reaction between CH_4 and O_2.

3.3 Performance of Catalysts for O_2 Removal

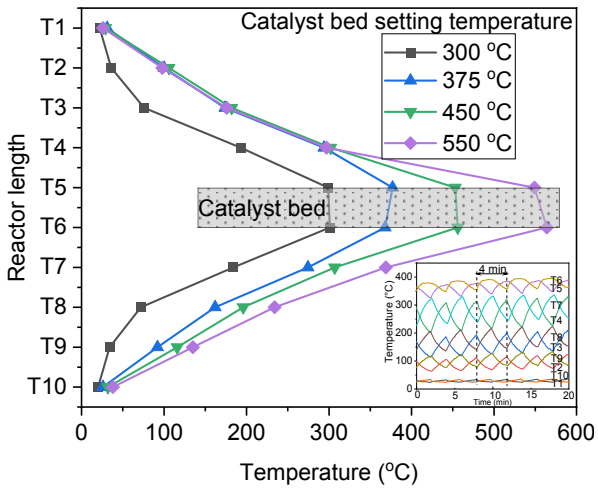

Fig. 4 Temperature profile snapshots over time along the length of the tubular reactor, and an exemplary temperature profile during a reverse-flow cyclic operation. (Catalyst: Cu 58 wt %/ZnO-Al_2O_3; Gas feed: 3% O_2, 1.5% CH_4, and balance CO_2; Reverse-flow cycle time: 4 min; Total pressure: 15 bar; GHSV: 18,000 h^{-1})

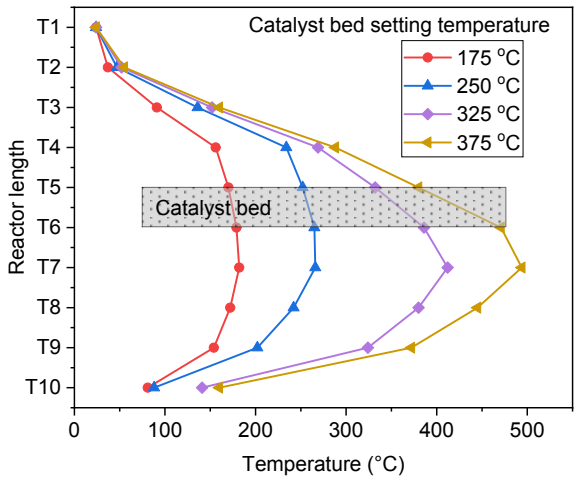

Fig. 5 Temperature profiles over time along the length of the tubular reactor under a one-direction flow operation. (Catalyst: Cu 58 wt. %/ZnO-Al_2O_3; Gas feed: 3% O_2, 1.5% CH_4, and balance CO_2; Total pressure: 15 bar; GHSV: 18,000 h^{-1})

The removal rates of residual O_2 in relation to the reaction temperature for different catalysts are plotted in Fig. 6. The experiments were conducted at 15 bar, a reverse-flow cycle time of 4 min, an O_2/CH_4 ratio of 2 (stoichiometric), and a GHSV of 18,000 h^{-1}. For each catalyst, the conversions of O_2 and CH_4 largely agreed with each other, suggesting complete oxidation of CH_4 to CO_2. The conversion of O_2 exhibited a sigmoidal growth trend with increasing temperature: The reaction lit off when a threshold temperature was reached, accelerated rapidly with increasing temperature, and reached near complete depletion of O_2 and CH_4 at high temperatures.

High catalytic activity led to high O_2 removal at low temperatures. Among the tested catalysts, $Co_{40}Mn_1$ and $Co_{20}Mn_1$ demonstrated the best catalytic activity. For both CoMn catalysts, the reaction lit off at ~350 °C and reached a 90% O_2 conversion at 425 °C. At approximately

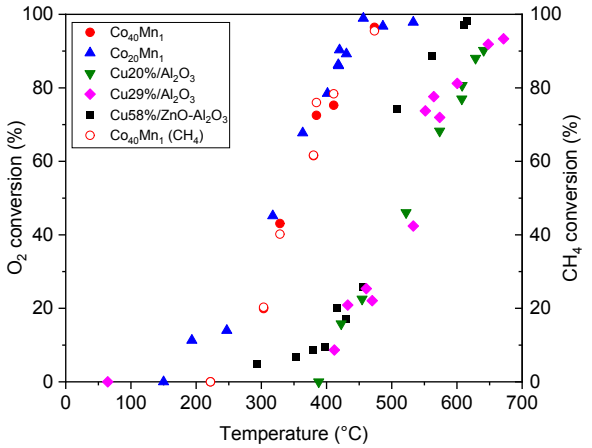

Fig. 6 Conversions of O_2 (solid) and CH_4 (open) as a function of the reaction temperature. (Catalysts: red circles: $Co_{40}Mn_1$, blue triangles: $Co_{20}Mn_1$, green triangles: Cu 20 wt %/Al_2O_3, purple diamonds: Cu 29 wt %/Al_2O_3, and black squares: Cu 58 wt %/ZnO-Al_2O_3; Gas feed: 3% O_2, 1.5% CH_4, and balance CO_2; Total pressure: 15 bar; GHSV: 18,000 h^{-1}; Flow pattern: reverse flow with a cycle time of 4 min)

500 °C, 99% of the O_2 in the feed gas was removed. Under the same conditions, for either Cu29%/Al_2O_3 or Cu20%/Al_2O_3, the reaction did not light off until 540 °C, and a 90% O_2 conversion was achieved when the temperature reached as high as 640 °C. As shown in Fig. 6, the four synthesized catalysts followed this order of activity from high to low: $Co_{40}Mn_1 \approx Co_{20}Mn_1 >> Cu20\%/Al_2O_3 > Cu29\%/Al_2O_3$. Although Cu20%/$Al_2O_3$ contained less copper than Cu29%/Al_2O_3, it exhibited the same Cu crystallite size (29 nm, Table S2) and a greater BET surface (102 vs. 91 m^2/g), which likely allowed for the exposure of more active Cu sites and led to higher activity. The commercial catalyst, Cu58%/ZnO-Al_2O_3, exhibited lower activity than the two CoMn catalysts but was slightly more reactive than the two synthesized Cu-based catalysts. Note that the particle size of the as-received Cu58%/ZnO-Al_2O_3 was larger than that of other catalysts. If the catalyst were reduced to the same particle size, less diffusion resistance would have been incurred and the measured activity might have been greater when the reaction accelerated at high temperatures (e.g., >450 °C).

All the tested catalysts under either a stoichiometric or CH_4-rich condition (e.g., O_2/CH_4 of 1.5 to 2.0) exhibited superior selectivity toward the complete redox reaction product CO_2, with negligible formation of partial CH_4 reduction products such as CO and H_2. In all the experiments, the concentrations of CO in the effluent gas streams never exceeded 30 ppmv and no H_2 was ever detected (Fig. S4), even when the O_2 feed was deficient for the complete reaction or at the highest temperatures tested (i.e., ~550 °C tested for the CoMn catalysts and ~650 °C for the Cu/Al_2O_3 catalysts). Under the CH_4-rich conditions, excess CH_4 simply slipped over without other reactions. According to Bahlawane,[13] partial oxidation of CH_4 over some cobalt-based catalysts does not likely occur at less than 750 °C. At higher temperatures, cobalt oxides become unstable, and CH_4 starts to be partially oxidized, generating CO at a slow rate. In the present study, the CoMn catalysts were not exposed to temperatures greater than 550 °C, and both were in the more stable form of $Co_xMn_{3-x}O_4$ (where x = 2.8 to 3) rather than Co_2O_3, as

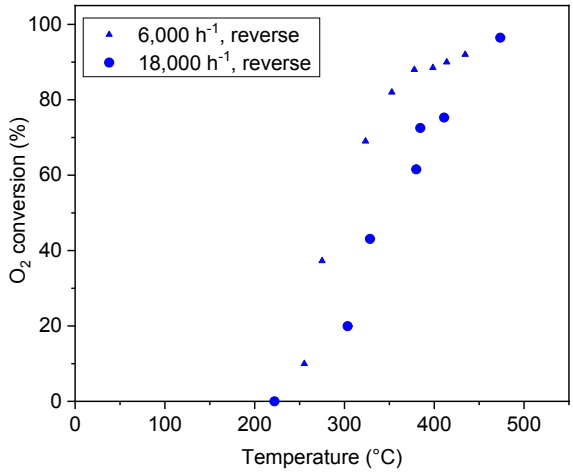

Fig. 7 Impact of GHSV on the conversion of O_2 at various temperatures. (Catalyst: $Co_{40}Mn_1$; Gas feed: 3% O_2, 1.5% CH_4, and balance CO_2; Total pressure: 15 bar; GHSV: triangles at 6,000 h^{-1} and circles at 18,000 h^{-1}; Flow pattern: reverse flow with a cycle time of 4 min)

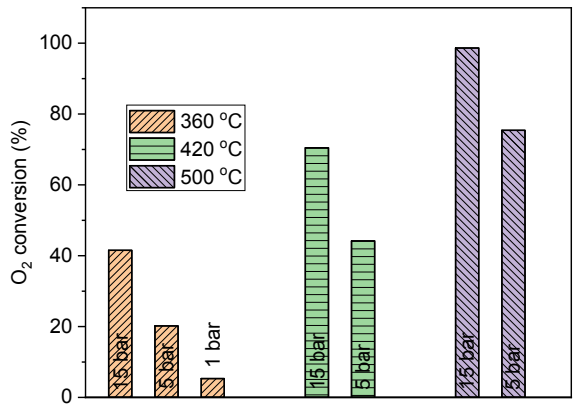

Fig. 8 Conversions of O_2 under different operating pressures (Catalyst: $Co_{40}Mn_1$; Gas feed: 3.0% O_2, 1.5% CH_4, and balance CO_2; Total pressure: 5 or 15 bar; GHSV: 18,000 h^{-1}; Flow pattern: one-direction flow)

previously determined from the XRD spectra. High selectivity was expected for the Cu-based catalysts based on our previous investigation.[23]

To investigate the effect of GHSV on the reaction, the $Co_{40}Mn_1$ catalyst was tested at GHSVs of 18,000 and 6,000 h^{-1} (Fig. 7). As expected, a smaller GHSV, corresponding to a longer residence time, led to a higher O_2 conversion. For example, in the reverse-flow experiment under 15 bar, the O_2 conversion at a GHSV of 18,000 h^{-1} reached only 43% at 325 °C, whereas that at a GHSV of 6,000 h^{-1} increased to 69%.

Operating pressure affects both the partial pressures of gas components and the gas residence time in the reactor when the gas mass flow rate remains the same. Higher partial pressures of the gas components or a longer residence time will result in greater adsorption of gas molecules on the active sites of the catalyst surface, thus facilitating the surface reactions. For the $Co_{40}Mn_1$

catalyst at a GHSV of 18,000 h^{-1} (Fig. 8), the O_2 conversion increased from 20% to 42% at 360 °C, from 44% to 77% at 420 °C, and from 75% to 99% at about 500 °C when the pressure was increased from 5 to 15 bar. The results clearly demonstrated that the reaction of O_2 reduction was favored at high-pressure conditions.

Note that despite the parametric assessment described above, no special effort was made to adjust the operating or gas feed conditions (e.g., by increasing the temperature or CH_4 injection) to reduce residual O_2 to exactly <100 ppmv in this study. However, the observed trend of O_2 removal in relation to these parametric conditions, as discussed previously, indicates it is possible to achieve such a level of O_2 purity.

3.4 Kinetics of O_2 Reduction with CH_4

To investigate the kinetics of the O_2 reduction reaction with CH_4, the RFFB reactor was purposely operated in a one-direction flow mode to allow the kinetic measurements to be conducted under a steady state. To maintain quasi-differential reaction conditions, the measurements were performed at 325 °C for the $Co_{40}Mn_1$ catalyst to ensure low conversions and thus relatively constant concentrations of the reactants. Low reaction rates at the low temperature also minimized the effect of diffusion on the overall reaction. The overall kinetic performance of the catalysts was further assessed at higher temperatures to investigate the effect of diffusion when the intrinsic reaction accelerated. The operation in a reverse-flow mode is dynamic in nature, which was not preferable for the kinetic study.

Effect of O_2 concentration. The performance of the $Co_{40}Mn_1$ catalyst was tested at 325 °C under different O_2/CH_4 ratios in the feed gas to create different redox atmospheres. In the experiments, the concentration of feed O_2 was varied from 1.5% to 3.75%, whereas that of CH_4 was kept constant at 1.5%. Under the constant operating pressure of 15 bar, varying the O_2 concentrations resulted in changing the partial pressures of O_2 from 22.5 to 56.3 kPa. As shown in Fig. 9, under such conditions, a change in feed O_2 concentration did not result in a noticeable change in the amount of reacted O_2, which remained at ~0.68 mol/mol of CH_4. The results indicated that the reaction was zero order with respect to the concentration of O_2.

Effect of CH_4 concentration. Similar experiments at 325 °C were also performed by varying the CH_4 concentrations from 1.2% to 2.0% in the feed gas while keeping the O_2 feed concentration constant. At 15 bar and 3% O_2 in the feed gas, the amount of reacted CH_4 increased consistently with an increase in CH_4 concentration (Fig. 9). For example, for the $Co_{40}Mn_1$ catalyst, the amount of reacted CH_4 was only 0.14 mol/mol of O_2 with 1.2% CH_4 in the feed gas; this amount increased to 0.17 mol/mol of O_2 with 1.5% feed CH_4 and further increased to 0.20 mol/mol of O_2 with 2.0% feed CH_4 in the feed gas. Such a linear trend contrasted with that observed for the reacted O_2, which was almost independent of the O_2 partial pressure under the tested conditions described above. Therefore, the reaction was first order with respect to the concentration of CH_4.

Reaction kinetics. The reaction rate between CH_4 and O_2 can be generally approximated by the following empirical equation:

$$-r = k_1 C_{CH4}^{\alpha} C_{O2}^{\beta} \quad (2)$$

where r is the reaction rate, k_1 is the rate constant, C is the concentration, and α and β are the exponential constants. Because

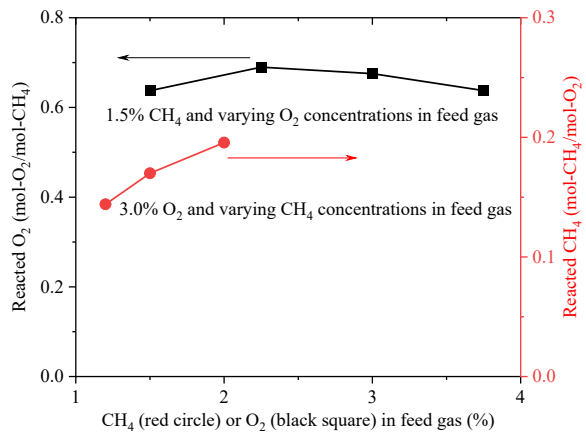

Fig. 9 Reacted amounts of O_2 or CH_4 at different O_2 or CH_4 concentrations in the feed gas. (Catalyst: $Co_{40}Mn_1$; Temperature: 325 °C; Gas feed: as labeled, and balance CO_2; Total pressure: 15 bar; GHSV: 18,000 h^{-1}; Flow pattern: one-direction flow)

the reaction was determined to be first order in CH_4 and zero order in O_2, eq (2) can be simplified to

$$-r = k_2 C_{CH4} \quad (3)$$

or

$$-r = k_3(1-X) \quad (4)$$

where X is the conversion of CH_4 and k_2 and k_3 are the modified rate constants. Note that the conversion or concentration of CH_4 is proportional to that of O_2, as they reacted almost at the stoichiometric ratio of 1:2 in all experiments.

Integrating eq (4) gives

$$k_3 = \frac{F}{V}\ln\frac{1}{1-X} \quad (5)$$

where F is the total flow rate and V is the volume of the catalyst bed.

Applying the Arrhenius equation gives

$$k_3 = Ae^{\frac{-E_a}{RT}} \quad (6)$$

where A is the pre-exponential factor, E_a is the activation energy, and R is the gas constant.

Combining eq (5) and eq (6) and differentiating each side of the combined equation with respect to $1/T$ gives

$$E_a = -R\frac{d\ln\ln\frac{1}{1-X}}{d\left(\frac{1}{T}\right)} \quad (7)$$

By plotting $\ln\ln[1/(1-X)]$ versus $1/T$ using the experimental data obtained at $T \leq 325$ °C (i.e., $1/T \geq 0.0017$ K^{-1}), a linear Arrhenius plot was obtained for either CoMn catalyst (solid lines, Fig. 10), which verified the assumption of unity order in CH_4 and zero order in O_2.

For data-fitting purposes, the reaction with the Cu-based catalysts was assumed to follow the same kinetic expression as eq (7) and the data obtained at $T \leq 500$ °C ($1/T \geq 0.0013$ K^{-1}) can also be illustrated by three solid lines in Fig. 10. The results of E_a for the five catalysts tested based on the above analysis are summarized in Table 1. The E_a ranged between 81 and 91 kJ/mol for the two CoMn catalysts and between 91 and 108 kJ/mol for the three Cu-based catalysts. The lower E_a for the CoMn catalysts was consistent with the greater activity for O_2 removal observed in the experiments.

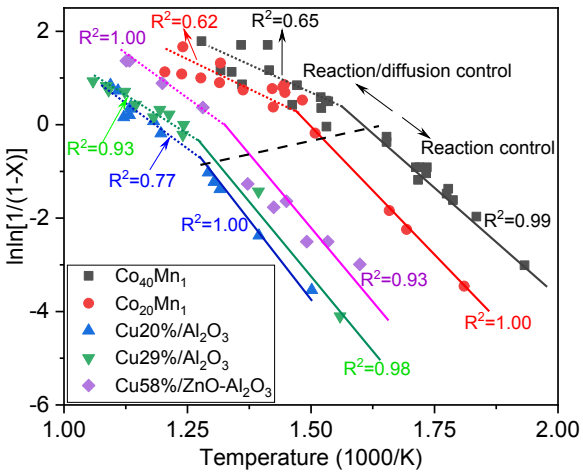

Fig. 10 Arrhenius plots for the tested catalysts (values of R^2 are labeled for each fitted line).

Reaction mechanism. Several possible reaction mechanisms[13,31] were examined, and the Mars–van Krevelen redox mechanism[13,32-34] was identified as valid to describe the experimental data obtained. According to this mechanism, the reaction proceeded in two steps. In the first step, lattice oxygen of the CoMn catalyst reacted with gaseous CH_4, which led to the reduction of lattice sites and the formation of oxygen-vacant sites on the catalyst surface. The second step involved the reaction between oxygen-vacant sites and gaseous O_2, resulting in reoxidation of the partially reduced lattice and the regeneration of lattice oxygen. The reaction pathway for the reaction between CH_4 and O_2 can thus be depicted as follows:

I: CH_4 + $[O]_{lattice}$ in oxidized catalyst $\xrightarrow{k_{red}}$ CO_2 + H_2O + Reduced catalyst with vacant lattice

II: O_2 + Reduced catalyst with vacant lattice $\xrightarrow{k_{ox}}$ $[O]_{lattice}$ in oxidized catalyst

Under the present experimental conditions (i.e., a pressure of 15 bar and the simulated oxy-combustion flue gas), the reaction between CH_4 and lattice oxygen of the CoMn catalyst (Step I) is the rate-limiting step, whereas the reaction between gaseous O_2 and the reduced CoMn catalyst (Step II) is a rather rapid process. This suggests that the surface of the CoMn catalyst was readily covered with oxygen. Because the reaction between CH_4 and lattice oxygen is slow, incorporating a small amount of Mn into the catalyst is considered beneficial for enhancing the adsorption of oxygen species on the catalyst surface and thus facilitating the O_2–CH_4 reaction.[16]

The reaction orders of unity in CH_4 and zero in O_2 determined from the above analysis also agreed with those reported in the literature.[13,31] In this study, the O_2 partial pressure in the feed gas varied from 22.5 to 56.3 kPa (1.5 to 3.75 vol % at a total pressure of 15 bar). In comparison, Belessi et al.[31] found that the reaction order in CH_4 was within 0.7–0.8 for CH_4 oxidation with perovskite catalysts. However, the reaction order in O_2 was reported at only 0.1–0.4 at lower O_2 partial pressures, and it gradually decreased to near zero when the O_2 partial pressure was increased to approximately 10 kPa. Bahlawane[13] observed that the reaction order in O_2 could be as high as 0.46 at O_2 partial pressures lower than 2 kPa but that it decreased to less than 0.02 at O_2 partial pressures above 40 kPa. The author also reported that the reaction order in CH_4 was always near unity.

Diffusion effect at higher temperatures. The form of eq (7) also applies for a first order reaction when the effect of diffusion is present and the apparent Ea is used in the equation.[35] Linear Arrhenius plots were observed by plotting $\ln\ln[1/(1-X)]$ versus $1/T$ using the experimental data obtained at higher temperatures of >325 °C for CoMn and >500 °C for the Cu-based catalysts (dotted fitting lines in Fig. 10), indicating that the overall first order reaction mechanism did not change at higher temperatures. The values of E_a estimated from the slopes of the lines are 42 kJ/mol for $Co_{40}Mn_1$, 42 kJ/mol for $Co_{20}Mn_1$, 72 kJ/mol for Cu20%/Al_2O_3, 48 kJ/mol for Cu29%/Al_2O_3, and 55 kJ/mol for Cu58%/ZnO-Al_2O_3, ranging from 44% to 73% of those of their counterparts at lower temperatures (Table 1).

Decreases in E_a estimated at higher temperatures indicated that the reaction was affected by both the intrinsic reaction and diffusion at higher temperatures compared with the dominance of the intrinsic reaction at lower temperatures.[36] Therefore, the estimated values of E_a at high temperatures were not intrinsic but apparent. Assuming a porous catalyst simplified with a uniform pore size (or average pore size), the relationship between the intrinsic E_a and the apparent E_a is given by eq (8)[35]:

$$E_{a,\,apparent} = 1/2\ E_{a,\,diffusion} + 1/2\ E_{a,\,intrinsic} \quad (8)$$

$E_{a,apparent}$ represents the intrinsic E_a only when there is no porous diffusion effect. If the overall reaction is controlled by diffusion, $E_{a,apparent}$ is roughly half of its intrinsic E_a because $E_{a,diffusion}$ is generally one order of magnitude smaller than $E_{a,apparent}$.[35] The observation that the apparent E_a at higher temperatures was 44% to 74% of the intrinsic E_a suggests that pore diffusion played an important role for all the catalysts tested at higher temperatures.

4. Conclusions

A laboratory fixed-bed reactor was successfully operated at 15 bar for the removal of residual O_2 from a simulated oxy-combustion flue gas under either a reverse-flow or one-direction flow mode. Four nonnoble metal-based catalysts, including two CoMn oxide catalysts and two alumina-supported Cu catalysts, were synthesized and tested. A commercial alumina-supported Cu catalyst was tested as the reference. The active components of the CoMn oxide catalysts were identified as $Co_xMn_{3-x}O_4$ (where x = 2.8 to 3) and those of the Cu catalysts were identified as Cu and Cu_2O. Both the CoMn- and Cu-based catalysts exhibited excellent selectivity toward the complete O_2–CH_4 reaction, even at the high temperatures tested. Among these catalysts, the two CoMn catalysts were superior in both activity and selectivity, with the reaction lighting off at ~350 °C and with 99% O_2 removal achieved at 500 °C. Under the simulated oxy-combustion flue gas composition and pressure conditions, the rate of the O_2–CH_4 reaction with the CoMn catalysts was unity order in CH_4 and zero order in O_2, and the apparent E_a ranged from 81 to 91 kJ/mol. The reaction mechanism studies revealed that the Mars–van Krevelen redox mechanism could approximate the reaction pathway and that the reaction between CH_4 and catalyst lattice oxygen was the rate-limiting step.

Conflicts of interest

There are no conflicts to declare.

Acknowledgements

This research was supported by the U.S. Department of Energy/National Energy Technology Laboratory through Cooperative Agreement Number DE-FE0029161. However, neither the United States Government nor any agency thereof, nor any of their employees, makes any warranty, express or implied, or assumes any legal liability or responsibility for the accuracy, completeness, or usefulness of any information, apparatus, product, or process disclosed, or represents that its use would not infringe privately owned rights. Reference herein to any specific commercial product, process, or service by trade name, trademark, manufacturer, or otherwise does not necessarily constitute or imply its endorsement, recommendation, or favoring by the United States Government or any agency thereof. The views and opinions of the authors expressed herein do not necessarily state or reflect those of the United States Government or any agency thereof. The authors thank Susan Krusemark at the Illinois State Geological Survey for assistance in editing of the manuscript.

Notes and references

1 IPCC Special Report on Carbon Dioxide Capture and Storage, Cambridge University Press, Cambridge, 2005.
2 A. Gopan, B. M. Kumfer and R. L. Axelbaum, International Journal of Greenhouse Gas Control, 2015, 39, 390-396.
3 C. Khan, R. Amin and G. Madden, Egyptian Journal of Petroleum, 2013, 22, 225-240.
4 M. Woods, M. Matuszewski and R. Brasington, Advancing Oxycombustion Technology for Bituminous Coal Power Plants: An R&D Guide, Report NETL/DOE-2010/1405, U.S. DOE/NETL, 2012.
5 T. Peppel, D. Seeburg, G. Fulda, M. Kraus, U. Trommler, U. Roland and S. Wohlrab, Chemical Engineering & Technology, 2017, 40, 153-161.
6 P. Zhao, G. Zhang, Y. Sun and Y. Xu, Environmental Science and Pollution Research, 2017, 24, 15240-15253.
7 J. H. Lee and D. L. Trimm, Fuel Processing Technology, 1995, 42, 339-359.
8 F. Ortloff, J. Bohnau, F. Graf and T. Kolb, Applied Catalysis B: Environmental, 2016, 182, 375-384.
9 P. Gélin and M. Primet, Applied Catalysis B: Environmental, 2002, 39, 1-37.
10 S. Su and J. Agnew, Fuel, 2006, 85, 1201-1210.
11 Q. Zheng, S. Zhou, M. Lail and K. Amato, Industrial & Engineering Chemistry Research, 2018, 57, 1954-1960.
12 O. Moro, Y. Moro Oka, Y. Morikawa and A. Ozaki, Journal of Catalysis, 1967, 7, 23-32.
13 N. Bahlawane, Applied Catalysis B: Environmental, 2006, 67, 168-176.
14 T.-C. Xiao, S.-F. Ji, H.-T. Wang, K. S. Coleman and M. L. H. Green, Journal of Molecular Catalysis A: Chemical, 2001, 175, 111-123.
15 U. Zavyalova, P. Scholz and B. Ondruschka, Applied Catalysis A: General, 2007, 323, 226-233.
16 C. Shi, Y. Wang, A. Zhu, B. Chen and C. Au, Catalysis Communications, 2012, 28, 18-22.
17 G. Águila, F. Gracia, J. Cortés and P. Araya, Applied Catalysis B: Environmental, 2008, 77, 325-338.
18 A. N. Kuhn, Y. Ma, C. Zhang, Z. Chen, M. Liu, Y. Lu, and H. Yang, Nanocatalyst Energy Technology, 2020, 8, 1901213.
19 Y. S. H. Matros and G. A. Bunimovich, Catalysis Reviews–Science and Engineering, 1996, 38, 1-68.
20 G. K. Boreskov and Y. U. S. Matros, Catalysis Reviews, 1983, 25, 551-590.
21 P. L. Silveston, Sadhana, 1987, 10, 217-246.
22 A. Zagoruiko, Current Topics in Catalysis, 2012, 10, 113-129.
23 A. N. Kuhn, Z. Chen, Y. Lu and H. Yang, Energy Technology, 2019, 7, 1800917.
24 E. Vila, R. M. Rojas, J. L. Martín de Vidales and O. García-Martínez, Chemistry of Materials, 1996, 8, 1078-1083.
25 D. G. Wickham and W. J. Croft, Journal of Physics and Chemistry of Solids, 1958, 7, 351-360.
26 A. Restovic, E. Ríos, S. Barbato, J. Ortiz and J. L. Gautier, Journal of Electroanalytical Chemistry, 2002, 522, 141-151.
27 E. Rios, J. L. Gautier, G. Poillerat and P. Chartier, Electrochimica Acta, 1998, 44, 1491-1497.
28 H.-K. Lin, H.-C. Chiu, H.-C. Tsai, S.-H. Chien and C.-B. Wang, Catalysis Letters, 2003, 88, 169-174.
29 C.-W. Tang, C.-B. Wang and S.-H. Chien, Thermochimica Acta, 2008, 473, 68-73.
30 L. Samain, A. Jaworski, M. Edén, D. M. Ladd, D.-K. Seo, F. Javier Garcia-Garcia and U. Häussermann, Journal of Solid State Chemistry, 2014, 217, 1-8.
31 V. Belessi, A. Ladavos, G. Armatas and P. Pomonis, Physical Chemistry Chemical Physics, 2001, 3, 3856-3862.
32 P. Mars and D. W. van Krevelen, Chemical Engineering Science, 1954, 3, 41-59.
33 K.-I. Fujimoto, F. H. Ribeiro, M. Avalos-Borja and E. Iglesia, Journal of Catalysis, 1998, 179, 431-442.
34 J. G. McCarty and H. Wise, Catalysis Today, 1990, 8, 231-248.
35 O. Lelvenspiel, Chemical Reaction Engineering, 3rd edn., John Wiley & Sons, Inc., 1999, Chapter 18.
36 J. Ross, Contemporary Catalysis, 1st edn., Elsevier, 2018, Chapter 8.

